Progress in Natural Science: Materials International 2012;22(6):684–692

Chinese Materials Research Society

Progress in Natural Science: Materials International

www.elsevier.com/locate/pnsmi
www.sciencedirect.com

ORIGINAL RESEARCH

Hydrothermal synthesis of $AlPO_4$-5: Effect of precursor gel preparation on the morphology of crystals

Dan Li[a,b], Jianfeng Yao[a], Huanting Wang[a,*]

[a]*Department of Chemical Engineering, Monash University, Clayton, Vic 3800, Australia*
[b]*Environmental Engineering, School of Engineering and Information Technology, Murdoch University, Murdoch, WA 6150, Australia*

Received 29 July 2012; accepted 7 October 2012
Available online 9 January 2013

KEYWORDS

Aluminophosphate;
$AlPO_4$-5;
Stirring;
Elliptical structure;
Crater structure

Abstract This paper reports on the effect of precursor gel preparation on the microstructural formation of aluminophosphate-5 ($AlPO_4$-5) molecular sieves in the hydrothermal synthesis. The morphology of $AlPO_4$-5 crystal changed from sphere to ellipse with two symmetrical craters when the aluminophosphate precursor gel was prepared via dropwise addition of acid and TEA under strong stirring, and continuous stirring overnight during the gel aging process. The results also showed that both of well-crystallized spherical and elliptical $AlPO_4$-5 crystals covered by the fibrous crystals could be hydrothermally synthesized at 150 °C for 4 h or longer. The average particle size of spherical $AlPO_4$-5 samples was about 35–45 μm in diameter, whereas the elliptical $AlPO_4$-5 exhibited approximately 13 μm in width and 15 μm in length.

1. Introduction

Aluminophosphate $AlPO_4$-5 with an AFI structure is composed of alternating AlO_4 and PO_4 tetrahedrons, which form a framework with one-dimensional, electrically neutral cylindrical pores of uniform cross-section (7.3 Å) that are extended parallel to the long (*c*) axis of the crystal [1–3]. It is an important material in shape-selective catalysis [4], separation technology [5–7], and nonlinear optics [8]. Similarly to other types of molecular sieves, $AlPO_4$-5 crystals can be synthesized *via* different routes, such as hydrothermal synthesis [9–14] and microwave heating [2,15–18]. Some synthesis parameters, including the initial composition of precursor solutions, temperature and crystallization time, are crucial in controlling the morphology of resulting $AlPO_4$-5. Jiang et al. concluded that HF content, crystallization temperature and duration were essential in obtaining optically clear hexagonal rods [19]. The results in Utchariyajit's research showed that the morphology could be controlled by varying the composition of reaction mixture, the addition of HF acid, the crystallization time

*Corresponding author. Tel.: +61 3 9905 3449.
E-mail address: huanting.wang@monash.edu (H. Wang).

Peer review under responsibility of Chinese Materials Research Society.

ELSEVIER Production and hosting by Elsevier

1002-0071 © 2013 Chinese Materials Research Society. Production and hosting by Elsevier Ltd. All rights reserved.
http://dx.doi.org/10.1016/j.pnsc.2012.11.003

and temperature [16]. They successfully synthesized mesoporous $AlPO_4$-5 with a perfect rod-like AFI structure *via* a microwave heating technique. Without adding HF in the synthesis gel, Mintova et al. synthesized nanosized AFI crystals and in some cases the crystal size could be substantially decreased to 50 nm by varying the composition ratio of Al_2O_3:triethylamine (TEA):-P_2O_5:H_2O under microwave heating [2,17]. Fiber-like, hexagonal rod (barrel), pencil-like, hexagonal plate and cross-like $AlPO_4$-5 aluminophosphate were prepared by systematically changing the initial composition of precursor solution at 150 °C for 6 h [9]. $AlPO_4$-5 with novel morphologies of brooms and nano-fibers (about 3.8 μm and 70–200 nm in width, respectively) were hydrothermally synthesized by varying the precursor compositions [20]. Non-doped and 11 (Si, Co, Mg, Zn, Mn, Sn(II), Sn(IV), Cr, Fe, V and Zr) heteroatom-doped $AlPO_4$-5 samples were crystallized using *N*-methyldicyclohexylamine as a structure-directing agent. The particles were cylindrical or spherical agglomerates composed of needle- or rod-like crystals [13]. Very recently, Zhang et al. prepared silica-$AlPO_4$-5 with bullet-, flower-like and disk-shaped morphologies from neutral or alkaline hydrogels using acetic acid or HCl at 180 °C for 48 h [21]. However, there has been no report on the effect of precursor gel preparation process, e.g. controlling reagent addition and stirring [22], on the morphology of aluminophosphate molecular sieves.

In this work, we report our finding on controlling the morphology of $AlPO_4$-5 by varying the precursor gel preparation conditions. Two different morphologies including well-crystallized spherical aluminophosphate $AlPO_4$-5 particles and elliptical $AlPO_4$-5 crystals with two symmetrical craters were successfully obtained.

2. Experimental section

2.1. Synthesis of $AlPO_4$-5 crystals

The synthesis procedures are summarized in Scheme 1. Two different preparation routes were used to synthesize $AlPO_4$-5 crystals.

Route I: In a typical synthesis, 4.1 g of aluminum isopropoxide (98%, Aldrich) was hydrolyzed in 18 g of deionized water for 3–4 h under magnetic stirring. An amount of 3 g of phosphoric acid (85%, Aldrich) was then added without stirring, and the resulting solution was stirred and allowed to homogenize for 1 h. The structure-directing agent (triethylamine, 99%, Aldrich) was added into the above solution under no stirring, and then stirred for 10 min. The molar composition of the synthesis gel was 1.00 Al_2O_3:1.33 P_2O_5:1.20 TEA:205 H_2O. The precursor gel was allowed to stand still for 12 h at 25 °C, followed by transferring into Teflon-lined autoclave and heating for different periods (0.5, 1, 2, 4, 6 and 8 h). After the hydrothermal reaction, the samples were collected by washing with sufficient deionized water and drying at 80 °C overnight. In order to remove the organic template TEA, the samples were calcined in oxygen at 600 °C for 6 h with a heating rate of 1 °C/min. The samples were denoted as S-0.5, S-1, S-2, S-4, S-6 and S-8 on the basis of the hydrothermal synthesis time, 0.5, 1, 2, 4, 6 and 8 h, respectively.

Route II: The recipe in Route II was exactly the same as that in Route I. The addition method of phosphate acid and TEA in Route II was changed to the dropwise addition instead of one-off addition in Route I (Scheme 1). The resulting samples were calcined in oxygen to 600 °C for 6 h to remove the organic templates, and they were denoted as H-0.5, H-1, H-2, H-4, H-6 and H-8 when the hydrothermal synthesis time was 0.5, 1, 2, 4, 6 and 8 h, respectively.

2.2. Characterization

Scanning electron microscopy (SEM) images were taken with a JSM-6300 F microscope (JEOL). X-ray diffraction (XRD) patterns were measured on a Philips PW1140/90 diffractometer with Cu K_α radiation (25 mA and 40 kV) at a scan rate of 1°/min with a step size of 0.02°. Thermogravimetric analysis (TGA, Perkin Elmer, Pyris 1 analyzer) was performed

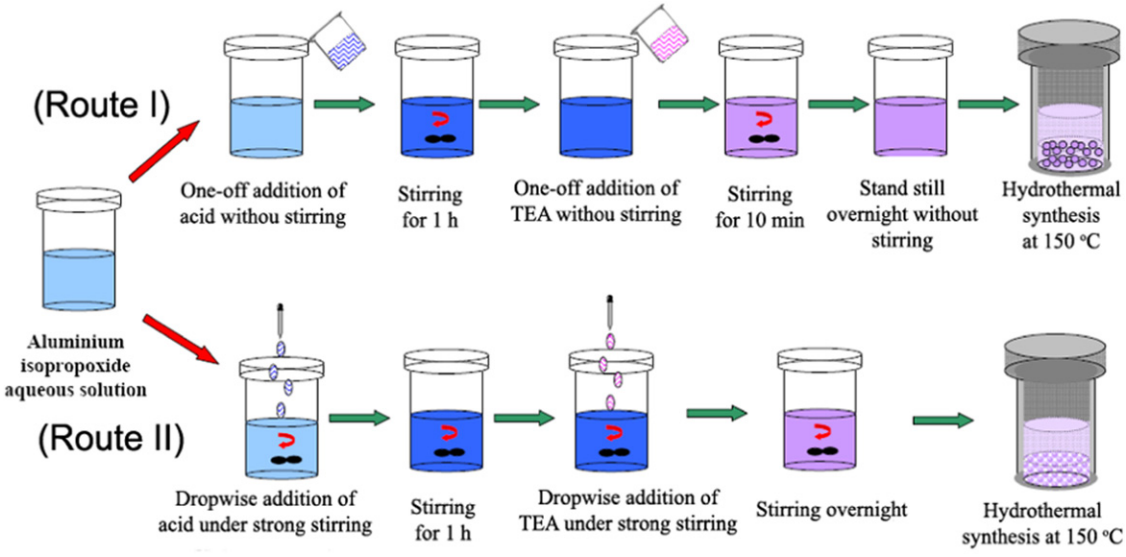

Scheme 1 Synthesis of $AlPO_4$-5 crystals *via* two different routes: one-off addition of reagents (acid and TEA) without stirring and no stirring in the aging process (Route 1); and dropwise addition of reagents with stirring, and continuous stirring in the aging process (Route 2).

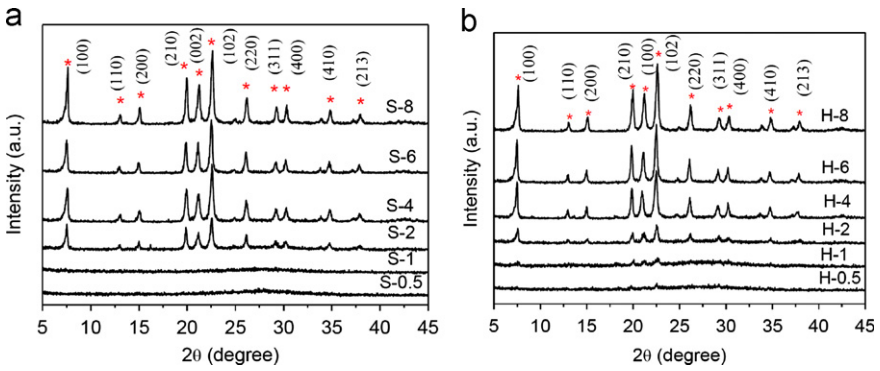

Fig. 1 XRD patterns of samples prepared *via* Route I (a) and Route II (b) by hydrothermal synthesis at 150 °C for 0.5–8 h. The peaks labeled with an asterisk arise from $AlPO_4$-5.

Table 1 Crystallite sizes of different samples, S-4, S-6, S-8, H-4, H-6 and H-8.

Samples	Crystallite size (nm)	Samples	Crystallite size (nm)
S-4	24.41	H-4	25.93
S-6	30.44	H-6	31.29
S-8	31.58	H-8	31.93

in oxygen at a heating rate of 5 °C/min to 800 °C. Nitrogen adsorption–desorption experiments were performed at 77 K with a Micrometritics ASAP 2020MC analyzer. The samples were degassed at 200 °C before analysis. The surface areas were determined by the Brunauer–Emmett–Teller (BET) method. The cross-section of the elliptical particle was prepared and examined with a FEI xT Nova Nanolab 200 DualBeam instrument, which combines dual beam high resolution focused ion beam (Ga FIB) miller and scanning electron microscope. The sample was directly attached onto conductive double side carbon tapes. To stabilize imaging with both electron and ion beams, a thin Au coating (about 25 nm thick) was sputtered on the specimen with an EmiTech K550x gold sputter coater. Selected area platinum deposition was conducted on the top surfaces of the particle within the FIB to protect $AlPO_4$-5 structures from the ion beam damage, and also minimize the mask effects of redeposition during the milling. The secondary electron images were taken at 52° tilt, which was the intrinsic milling position of the stage.

3. Results and discussion

Fig. 1 shows XRD patterns of the samples synthesized from the precursor gel with a molar ratio 1.00 Al_2O_3:1.33 P_2O_5:1.20 TEA:205.00 H_2O. The gels prepared by Routes I and II were hydrothermally synthesized at 150 °C for different periods (0.5–8 h). Both of the samples show amorphous structure after 0.5 h hydrothermal synthesis. After 1 h hydrothermal treatment, S-1 still appears to be amorphous, whereas H-1 exhibits a low crystallinity indicating the beginning of $AlPO_4$-5 crystallization. In Route II, the dropwise addition of reagents, e.g., acid and TEA, under strong stirring and the continuous stirring overnight in aging are expected to enhance a better dissolution and mixing of phosphoric acid, aluminum isopropoxide and organic template TEA, resulting in a more uniform precursor gel for hydrothermal reaction. All the other samples with a hydrothermal synthesis time over 4 h (S-4, S-6, S-8, H-4, H-6 and H-8) are well-crystallized $AlPO_4$-5. The intensities of $AlPO_4$-5 characteristic XRD peaks become greater with increasing the hydrothermal synthesis time. To further investigate the crystallization of samples prepared *via* two Routes after 4 h hydrothermal synthesis or longer, Table 1 summarizes their crystallite sizes based on the XRD patterns in Fig. 1a and b. The crystallite sizes were estimated on the basis of the broadening of XRD peaks using the Scherrer formula $D=k\lambda/B\cos\theta$, in which D is the crystallite size (nm), k is the wavelength of Cu K_α radiation (0.1541 nm), and B is the calibrated width of diffraction peak at the half-maximum intensity. The crystallite sizes of samples increase with increasing the hydrothermal time. In particular, at the same hydrothermal time, the crystallite sizes of H samples prepared *via* Route II are slightly larger than those synthesized from Route I. After 8 h hydrothermal synthesis, the average crystallite sizes of S-8 and H-8 are 31.58 and 31.93 nm, respectively. It suggests that the precursor gel preparation by dropwise adding reagents under strong stirring and continuous stirring overnight likely affects early crystallization more than prolonged crystallization ($\geq$4 h).

Fig. 2 shows the TGA and differential thermogravimetric (DTG) curves of samples, (a) S-2 and H-2 and (b) S-8 and H-8 which were calcinated up to 800 °C. There is a main mass loss before 100 °C for all of the samples. It is mainly attributed to the loss of adsorbed water. The other main DTG peak is between 150 and 200 °C and the corresponding mass loss is mainly related to the decomposition and oxidation of organic template TEA in $AlPO_4$-5. Interestingly, the DTG peak for the sample prepared *via* Route II (*e.g.* H-2 and H-8) is centered at around 190 °C, which is higher than that for the samples made in Route I (*e.g.* S-2 and S-8) that is centered at approximately 175 °C. This may be explained by the effect of precursor gel preparation, including dropwise addition of reagents under strong stirring and continuous stirring overnight for aging, which makes TEA disperse thoroughly in the preparation of the precursor gel. The mass residues of S-8 (Route I) and H-8 (Route II) with the organic templates, are 88.3% and 86.5%, respectively, both of which are more than those of S-2 (Route I) and H-2 (Route II) with the organic templates, 77.40% and 71.64%, due to the crystal growth after the prolonged hydrothermal synthesis. These results also indicate that more

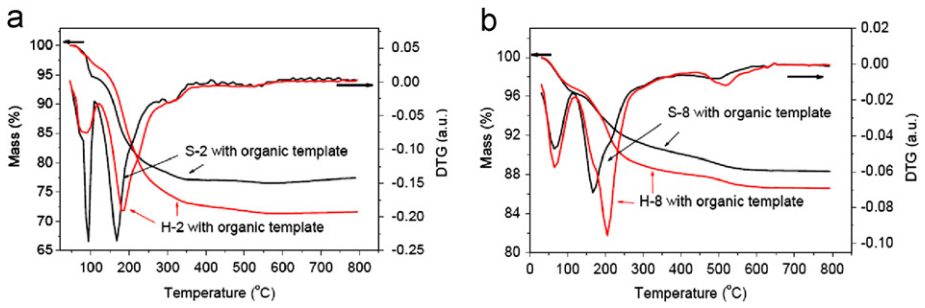

Fig. 2 TGA and DTG curves of the samples prepared via Routes I and Route II, (a) S-2 and H-2 and (b) S-8 and H-8.

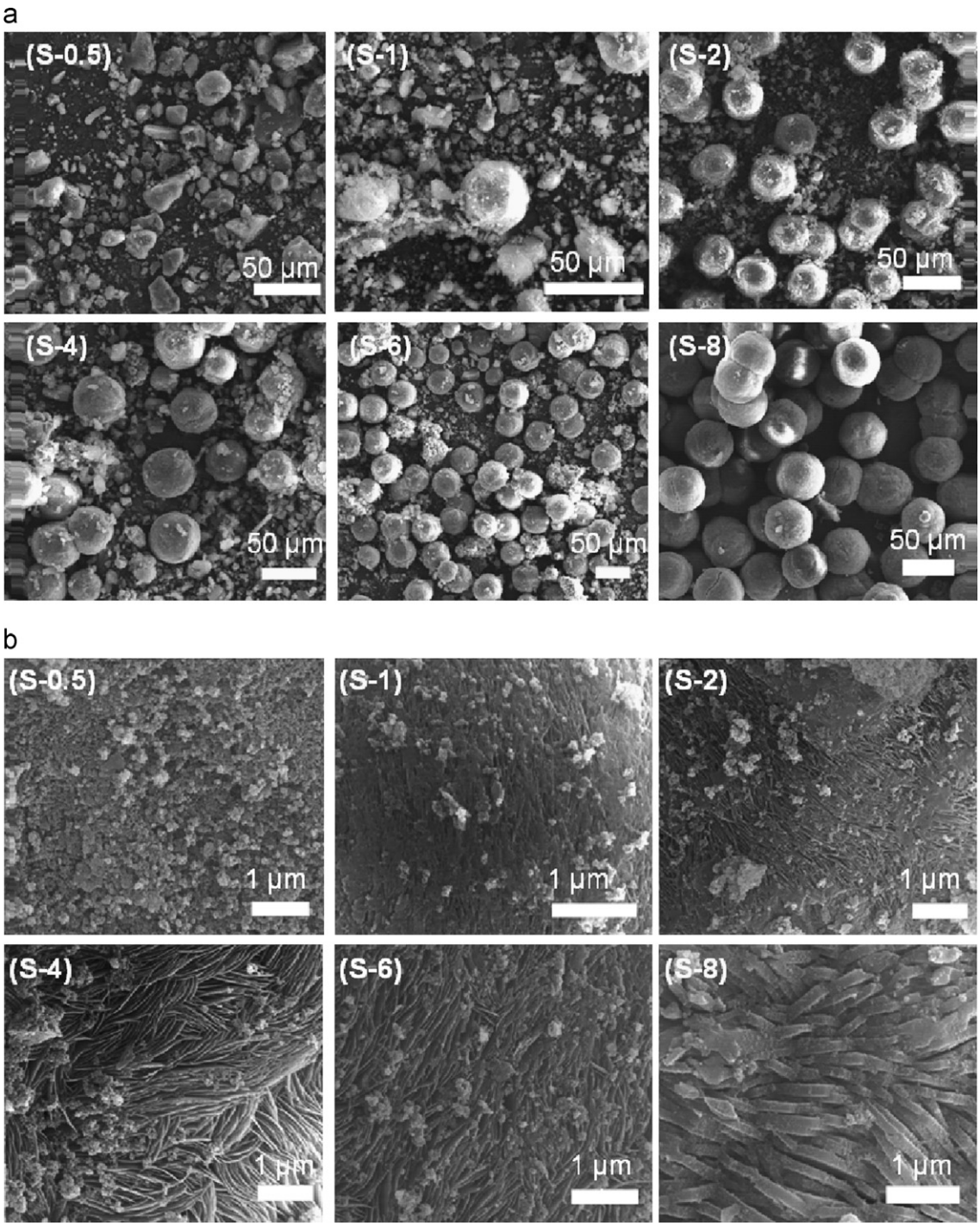

Fig. 3 SEM images of samples prepared with Route I by hydrothermal synthesis at 150 °C for different times, S-0.5, S-1, S-2, S-4, S-6, and S-8, at low magnification (a) and high magnification (b).

TEA is trapped in the $AlPO_4$-5 prepared *via* Route II as compared with that *via* Route I.

Figs. 3 and 4 show SEM images of the samples synthesized from the precursor gels that were prepared by Route I/II and hydrothermally synthesized for 0.5–8 h. By using Route I, Fig. 3a shows some small amorphous particles being aggregated to large blocks (S-0.5) after 0.5 h hydrothermal synthesis. When the synthesis time is extended to 1 h, a small amount of spherical particles (S-1) with a size of about 35 μm (Fig. 3a) are obtained, and the particles are covered by a fibrous structure (Fig. 3b). For the samples S-2, S-4, S-6 and S-8 (Fig. 3a), all of the particles exhibit a spherical morphology and the particle sizes range from 35 μm to 45 μm. From the high magnification images (Fig. 3b), it is clear that the morphology of particle surface is substantially affected by increasing hydrothermal reaction time. The width of $AlPO_4$-5 fibrous structure on the particle surface increases from around 24 nm for S-2 to 150 nm for S-8, which should be due to the aluminaphosphate crystallization.

Similarly, by using Route II, there are some amorphous blocks composed of small particles with a size of about 100 nm

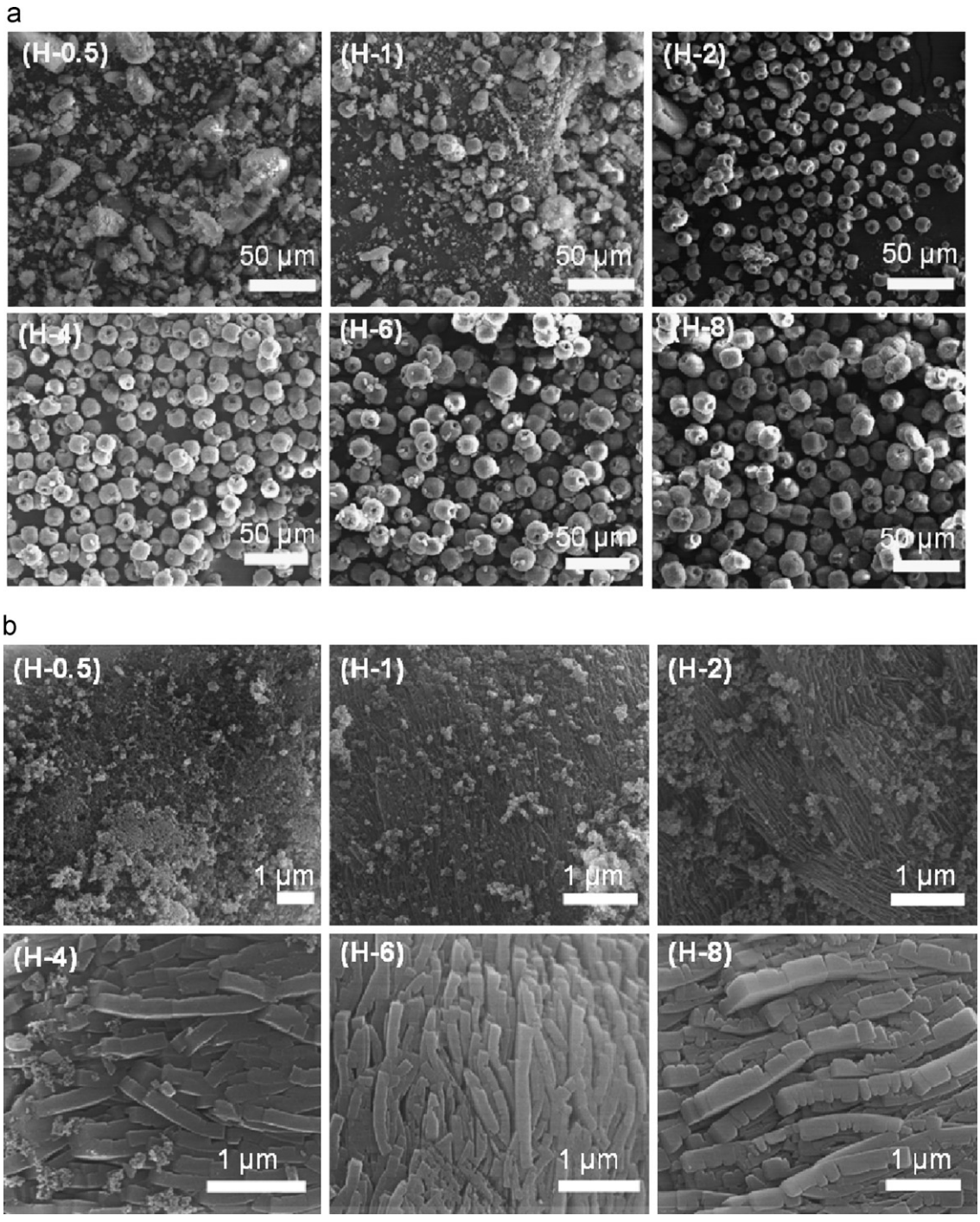

Fig. 4 SEM images of samples prepared with Route II by hydrothermal treatment at 150 °C for different times, H-0.5, H-1, H-2, H-4, H-6, and H-8, at low resolution (a) and high resolution (b).

after 0.5 h of hydrothermal synthesis (Fig. 4a). For H-1, H-2, H-4, H-6 and H-8 samples, the $AlPO_4$-5 crystals exhibit similar elliptical structure with craters. There is no significant change in both width and length of particles when the hydrothermal synthesis time increases from 1 to 8 h. However, the width of the outer surface fibrous structure increases from about 20 to 40 nm for H-2 to around 250 nm for H-8 (Fig. 4b).

The morphology of samples prepared by Route II appears differently from those in Route I. The morphologies (Fig. 5) of samples prepared by Route I (S-8) and Route II (H-8) were further examined by SEM and FIB–SEM. Fig. 5a shows an intact and spherical $AlPO_4$-5 particle, having a size of about 35 μm. However, Fig. 5b and c shows the H-8 particles with an elliptical structure and two symmetrical craters (~5.4 μm in diameter) on the surface. The particle size of H-8 is around 13 μm in width and 15 μm in length, both of which are smaller than the size of S-8. Its top view shows a hexagon shape (Fig. 5c), which is consistent with previously reported characteristic shape of well-crystallized $AlPO_4$-5 [19,23]. To further investigate the internal structure of H-8, the FIB–SEM image of the cross-section shows a solid core in center (Fig. 5e).

To investigate the pore structures of the samples synthesized from the precursor gels that were prepared by Routes I and II, Fig. 6 shows nitrogen adsorption–desorption isotherms and DFT pore size distributions of S-8 and H-8 before and after the removal of organic templates by calcination. The BET-specific surface areas of uncalcined spherical (S-8) and elliptical (H-8) $AlPO_4$-5 are 8.6 and 10.5 m^2/g, respectively. Furthermore, both of N_2 sorption isotherms in Fig. 6 show hysteresis loops. The DFT pore size distributions indicate there are small amounts of pores (pore sizes ranging from 1 to 150 nm). These pores are mainly generated by the packing of the fibrous structure. Fig. 6 also shows N_2 sorption isotherms of the calcined S-8 and H-8. High adsorption capacities at very

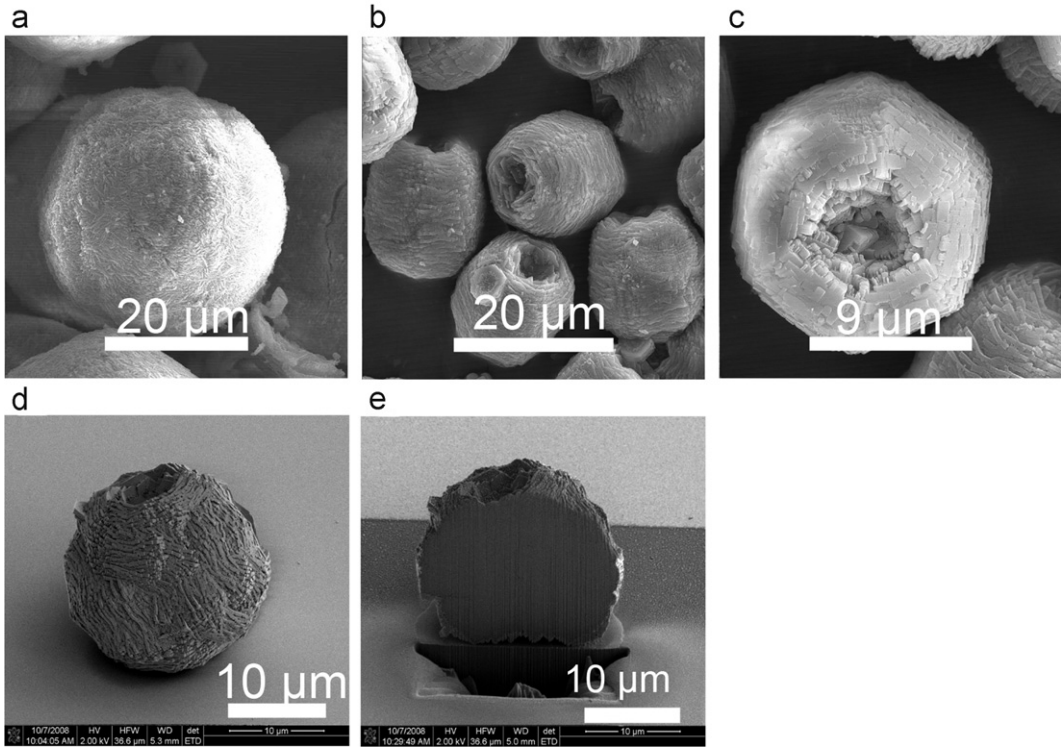

Fig. 5 SEM images of samples: S-8 (a) and H-8 (b,c), FIB–SEM images of the individual H-8 particle (d) and the cross-section (e).

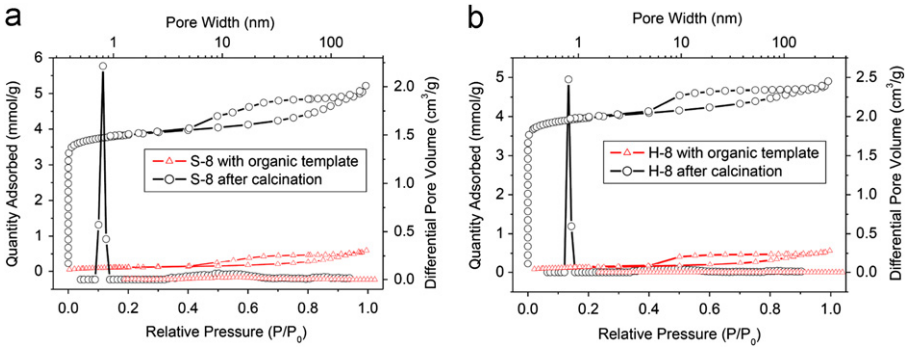

Fig. 6 Nitrogen adsorption–desorption isotherms and DFT pore size distributions of S-8 with and without organic template (TEA) (a), and H-8 with and without organic template (TEA) (b).

low pressures reveal the presence of microporous structure in these two samples. The BET-specific surface areas of calcined S-8 and H-8 are calculated to be 309 and 320 m^2/g, respectively, close to the reported surface area for a typical $AlPO_4$-5, suggesting that AFI pore structure are well developed in these two samples [24]. Very narrow pore-size distributions centered at around 0.75 nm (Fig. 6) with some mesopores are observed, which corresponds well with the reported value (0.73 nm) for AFI structure [2,25].

The evolution of crater elliptical $AlPO_4$-5 was further studied. Fig. 7 shows the SEM images of typical particles for H-0.5, H-1, H-2, H-4, H-6 and H-8. When the hydrothermal synthesis time is 0.5 h, only a limited number of particles are found, and the particles exhibit a spherical shape with a size of around 4 μm, where a very shallow crater structure seems to appear. The crater becomes clear after 1 h or a longer synthesis time. The precursor gel preparation process, such as dropwise addition of reagents under strong

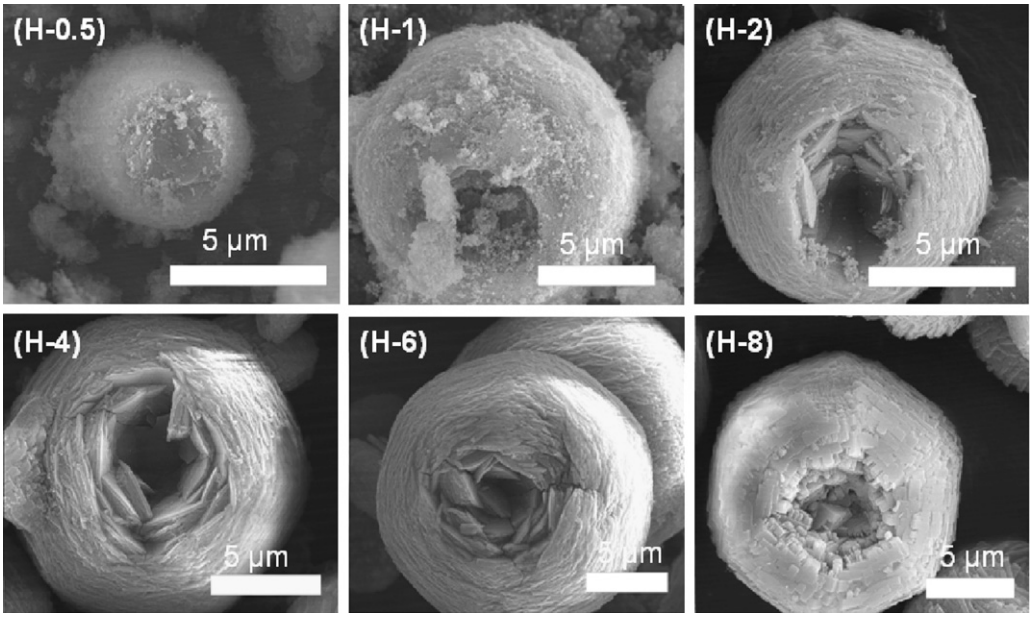

Fig. 7 SEM images of the individual particles from H-0.5, H-1, H-2, H-4, H-6 and H-8.

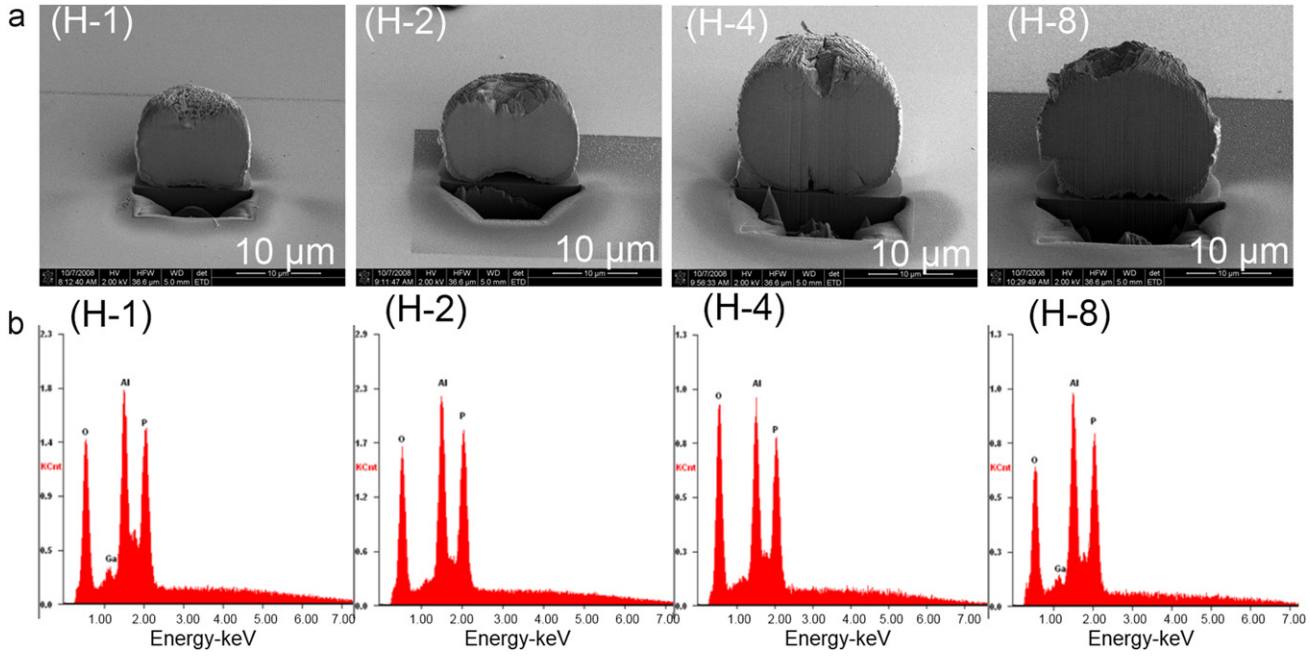

Fig. 8 FIB-SEM images of the cross-sections for samples H-1, H-2, H-4 and H-8 (a), and the EDX spectra of the cores of these samples (b).

stirring and continuous stirring overnight in the aging process (Route II), likely affects the mode of aggregation and assembly of nuclei, as compared with the sample which was prepared with no stirring and one-off addition of reagents, thus forming the particulates with different morphologies. Due to Oswald ripening, further hydrothermal synthesis leads to the dissolution of small particles in the gel solution and the subsequent redeposition onto large crystals. The apparent crater structures form as a result of prolonged crystallization in the hydrothermal synthesis. Moreover, the SEM images (Fig. 7) show that the width of outer surface fibrous structure becomes greater, whilst the crater size decreases with increasing the crystallization time. It can be related to the accessibility of precursor solution during the extended hydrothermal synthesis. It is noted that the precursors in the solution are a source of nutrition for crystal growth. The surface fibers are very easy to access to the nutrients in solution, thus further growing into wider crystals by extending hydrothermal synthesis duration. Furthermore, from the previous nitrogen adsorption–desorption results, it is found that there are some large pores in the samples, which can be the tunnels for precursor solution penetration. Meanwhile, the formed craters can also be open spaces for precursor solution to travel into the particles. Therefore, the internal crystals can further grow into big crystals. More importantly, the images show a shape change on the top view of the parties, from round to hexagon, which is the characteristic structure of $AlPO_4$-5 [19]. Fig. 8 exhibits the FIB–SEM images (a) of the cross-section for different samples, H-1, H-2, H-4 and H-8; and the corresponding elemental analysis results of their cores (b). They clearly indicate that the cores of all synthesized samples after 1 h or longer hydrothermal synthesis are pure $AlPO_4$-5 (Fig. 8b), which is consistent with the XRD result.

The effect of hydrothermal time on the formation of elliptical particle was further studied. The sample (denoted as H-24) was hydrothermally synthesized at 150 °C for 24 h (Fig. 9). Fig. 9a shows the XRD pattern that is exactly the same as H-8. There is no significant difference in particle size between H-24 and H-8 and the craters still can be observed in the sample H-24, but the depth of pores seems to be filled with some crystals (Fig. 9c). Furthermore, large plate-like crystals with a width of about 800 nm are covered on the surface (Fig. 9d).

4. Conclusions

$AlPO_4$-5 aluminaphosphate molecular sieves were hydrothermally synthesized from an $Al_2O_3/P_2O_5/TEA/H_2O$ system. The variation on the precursor gel preparation process resulted in

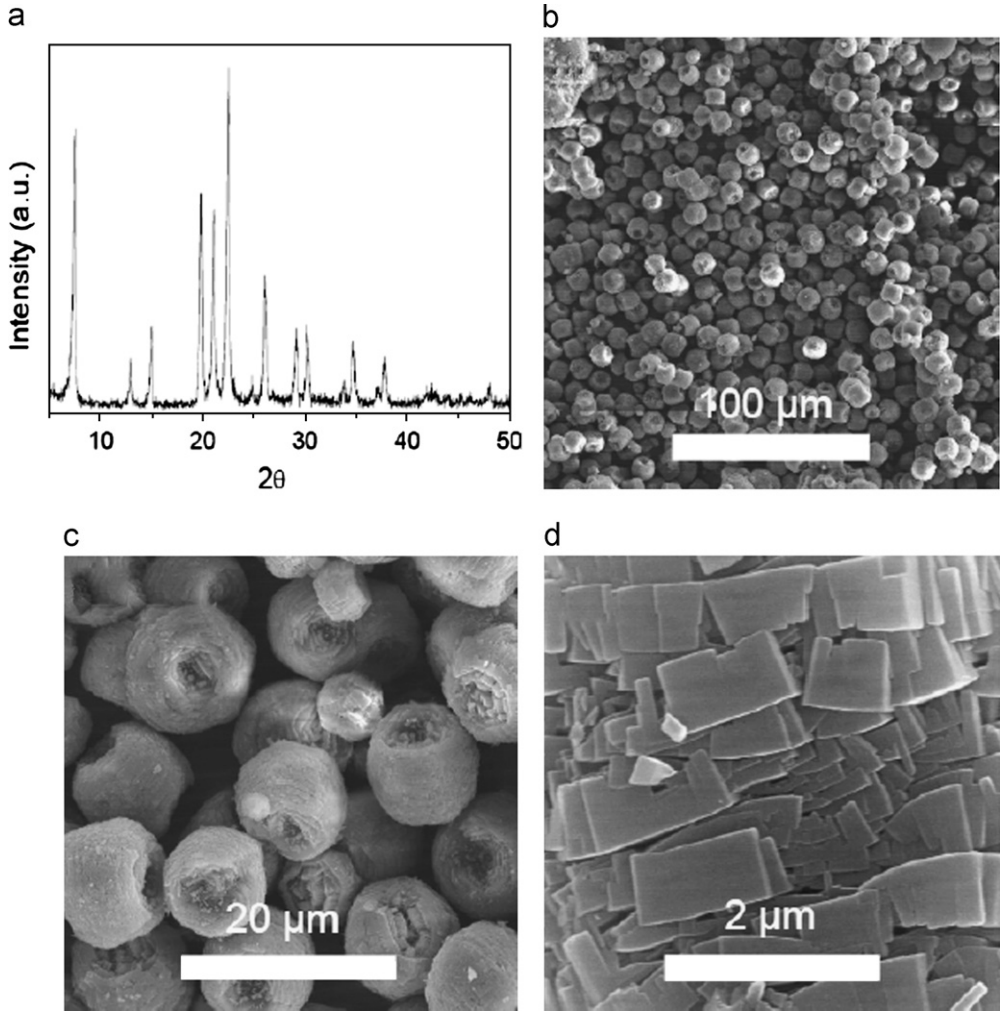

Fig. 9 XRD pattern (a) and SEM images (b–d) of the sample H-24 prepared by hydrothermal synthesis at 150 °C for 24 h.

the formation of $AlPO_4$-5 crystals with different morphologies: spheres and ellipses with two symmetrical craters. Well-crystallized spherical $AlPO_4$-5 crystals were synthesized after 4 h of hydrothermal synthesis at 150 °C from a precursor gel without stirring and one-off addition of phosphoric acid and organic template TEA. The individual particles had particle sizes ranging from 35 to 45 μm. Elliptical $AlPO_4$-5 crystals with two symmetrical craters were produced from an initial gel with strong stirring and dropwise addition of phosphoric acid and template TEA. There is no obvious change in the particle size of the elliptical $AlPO_4$-5 synthesized for different synthesis times. The craters remained even after 24 h hydrothermal synthesis at 150 °C. This study also provides a new insight into the understanding of $AlPO_4$-5 crystallization.

Acknowledgement

This work was supported by Monash University and the Australian Research Council. H.W. thanks the Australian Research Council for a Future Fellowship. J.Y. thanks Monash University for the Monash Fellowship.

References

[1] T. Kimura, Surfactant-templated mesoporous aluminophosphate-based materials and the recent progress, Microporous Mesoporous Materials 77 (2005) 97–107.
[2] S. Mintova, S. Mo, T. Bein, Nanosized $AlPO_4$-5 molecular sieves and ultrathin films prepared by microwave synthesis, Chemistry of Materials 10 (1998) 4030–4036.
[3] G.N. Karanikolos, J.W. Wydra, J.A. Stoeger, H. Garcia, A. Corma, M. Tsapatsis, Continuous c-oriented $AlPO_4$-5 films by tertiary growth, Chemistry of Materials 19 (2007) 792–797.
[4] Z.M. Li, J.P. Zhai, H.J. Liu, I.L. Li, C.T. Chan, P. Sheng, Z.K. Tang, Synthesis of 4 Å single-walled carbon nanotubes in catalytic Si-substituted $AlPO_4$-5 molecular sieves, Applied Physics Letters 85 (2004) 1253–1255.
[5] C.K. Choo, K. Enomoto, K. Tanaka, Size selective filtration of silicon nano-structures using AFI $AlPO_4$-5 zeolite pores, Materials Science and Engineering B 104 (2003) 73–79.
[6] S.I. Ishimaru, K. Gotoh, M. Ichikawa, R. Ikeda, Dynamic behavior of acetonitrile molecules adsorbed in $AlPO_4$-5 and SAPO-5 studied by ^1H and ^2H NMR, Microporous Mesoporous Materials 51 (2002) 17–22.
[7] P. Adhangale, D. Keffer, A grand canonical Monte Carlo study of the adsorption of methane, ethane, and their mixtures in one-dimensional nanoporous materials, Langmuir 18 (2002) 10455–10461.
[8] S. Feng, T. Bein, Vertical aluminophosphate molecular sieve crystals grown at inorganic–organic interfaces, Science 265 (1994) 1839–1841.
[9] R. Xu, G. Zhu, X. Yin, X. Wan, S. Qiu, In situ growth of $AlPO_4$-5 molecular sieve on stainless steel support, Microporous Mesoporous Materials 90 (2006) 39–44.
[10] J.G. Longstaffe, B. Chen, Y. Huang, Characterization of the amorphous phases formed during the synthesis of microporous material $AlPO_4$-5, Microporous Mesoporous Materials 98 (2007) 21–28.
[11] M. Elanany, B.L. Su, D.P. Vercauteren, Strong templating effect of TEAOH in the hydrothermal genesis of the $AlPO_4$-5 molecular sieve: experimental and computational investigations, Journal of Molecular Catalysis A 270 (2007) 295–301.
[12] F.Y. Jiang, Z.K. Tang, J.P. Zhai, J.T. Ye, J.R. Han, Synthesis of $AlPO_4$-5 crystals using TBAOH as template, Microporous Mesoporous Materials 92 (2006) 129–133.
[13] A. Manjon-Sanz, M. Sanchez-Sanchez, P. Munoz-Gomez, R. Garcia, E. Sastre, Non-templated intercrystalline mesoporosity in heteroatom-doped $AlPO_4$-5 using *N*-methyldicyclohexylamine as structure-directing agent, Microporous Mesoporous Materials 131 (2010) 331–341.
[14] J. Kim, K. Biswas, K.W. Jhon, S.Y. Jeong, W.S. Ahn, Synthesis of $AlPO_4$-5 and CrAPO-5 using aluminum dross, Journal of Hazardous Materials 169 (2009) 919–925.
[15] I. Braun, M. Bockstette, D. Wöhrle, G. Schulz-Ekloff, Microwave-assisted crystallization inclusion of coumarin and AZO dyes in $AlPO_4$-5 molecular sieves, Zeolites 19 (1997) 128–132.
[16] K. Utchariyajit, S. Wongkasemjit, Structural aspects of mesoporous $AlPO_4$-5 (AFI) zeotype using microwave radiation and alumatrane precursor, Microporous Mesoporous Materials 114 (2008) 175–184.
[17] M. Fang, H. Du, W. Xu, X. Meng, W. Pang, Microwave preparation of molecular sieve $AlPO_4$-5 with nanometer sizes, Microporous Materials 9 (1997) 59–61.
[18] H. Shao, J.F. Yao, X.B. Ke, L.X. Zhang, N.P. Xu, Microwave-assisted fast vapor-phase transport synthesis of MnAPO-5 molecular sieves, Materials Research Bulletin 44 (2009) 956–959.
[19] F.Y. Jiang, J.P. Zhai, J.T. Ye, J.R. Han, Z.K. Tang, Synthesis of large optically clear $AlPO_4$-5 single crystals, Journal of Crystal Growth 283 (2005) 108–114.
[20] C.X. Zhao, Y.X. Yang, W. Chen, H.T. Wang, D.Y. Zhao, P.A. Webley, Hydrothermal synthesis of novel $AlPO_4$-5 brooms and nano-fibers and their templated carbon structures, CrystEngComm 11 (2009) 739–742.
[21] M. Li, C.F. Zeng, L.X. Zhang, Hydrothermal synthesis of SAPO-5 with novel morphologies from hydrogels containing acetic acid and high concentration of triethylamine under neutral or alkaline conditions, CrystEngComm 14 (2012) 3787–3792.
[22] D. Li, R.B. Kaner, Shape and aggregation control of nanoparticles: not shaken, not stirred, Journal of the American Chemical Society 128 (2006) 968–975.
[23] I. Girnus, K. Jancke, R. Vetter, J. Richter-Mendau, J. Caro, Large $AlPO_4$-5 crystals by microwave heating, Zeolites 15 (1995) 33–39.
[24] N. Murayama, N. Okajima, S. Yamaoka, H. Yamamoto, J. Shibata, Hydrothermal synthesis of $AlPO_4$-5 type zeolitic materials by using aluminum dross as a raw material, Journal of the European Ceramic Society 26 (2006) 459–462.
[25] J.C. Lin, M.Z. Yates, Growth of oriented molecular sieve thin films from aligned seed layers, Chemistry of Materials 18 (2006) 4137–4141.